



A grinding force prediction model for SiCp/Al composite based on single-abrasive-grain grinding

Peng Gu¹ · Chuanmin Zhu¹ · Zhan Tao¹ · Yiqing Yu¹

Received: 12 February 2020 / Accepted: 11 June 2020 / Published online: 17 July 2020
© Springer-Verlag London Ltd., part of Springer Nature 2020

Abstract

Grinding is the main processing method for particle-reinforced composites, and grinding force prediction models are very important for research on removal mechanisms. In this study, single-abrasive-grain grinding experiments on SiCp/Al composites were conducted to determine the grinding forces at different grinding process parameters. In addition, a prediction model for the single-abrasive-grain grinding force was established to study the influence of the grinding process parameters and grinding grain angle on the grinding force of SiCp/Al composite. Moreover, multi-abrasive-grain grinding experiments were conducted at different grinding process parameters, which resulted in different grinding forces. The support vector machine (SVM) prediction method based on particle swarm optimisation (PSO) was used to establish a prediction model for the multi-abrasive-grain grinding force; the single-abrasive-grain grinding forces at different grinding grain angles were the input, and the average experimental grain grinding force was the output. The results show that the error between the predicted and experimental grinding forces is below 12%. Furthermore, the grinding force decreases with increasing wheel speed and increases with increasing feed velocity and grinding depth. The PSO–SVM algorithm–based grinding force prediction model can accurately predict the grinding force of SiCp/Al composite and provides theoretical support for improved surface quality.

Keywords SiCp/Al composite · Single-abrasive-grain grinding · Grinding force prediction model · Grinding mechanism · PSO · SVM

1 Introduction

SiCp/Al composite is a typical particle-reinforced composite with a high elasticity modulus and low thermal expansion coefficient. It has become an important substitute for glass–ceramics and quartz glass and is widely used in the aerospace field. Grinding is the main processing method for particulate-reinforced composites. Therefore, developing a grinding force prediction model helps to investigate the removal mechanisms and usability performance after grinding.

Many researchers have studied the machining process of SiCp/Al composite. For example, Huang et al. [1, 2] milled SiCp/Al composite with polycrystalline diamond tools and discovered that a higher cutting speed mitigates the formation of built-up edges and scale-stabs. When the cutting speed is

increased, silicon carbide particles are pushed by the cutting edge and rear face, which causes defects such as cavities on the surface. Li et al. [3] studied the influence of the milling parameters of SiCp/Al composite on the milling force and surface roughness, and the processing conditions for high-quality SiCp/Al composite surfaces were determined. Moreover, Han et al. [4] discovered that polycrystalline diamond tools with chamfered edges protect cutting edges from damage; chamfered edges can effectively strengthen cutting edges, and a particle size of polycrystalline diamond of 2–30 μm leads to higher milling surface quality. Wang et al. [5] studied the precision turning mechanism of SiCp/Al composite with a volume fraction of 30%; the results show that when the tool acted on top and mid-section particles, they usually fractured along the direction of the stress concentration. When the tool acted on bottom particles, they were easily pulled out from the material matrix, which affected the turning surface quality of the SiCp/Al composite. Furthermore, Xie et al. [6–8] used diamond tools to drill SiCp/Al composite with a volume fraction of 65% and studied the effects of the drilling speed, drilling depth, and front angle on the drilling

✉ Chuanmin Zhu
01065@tongji.edu.cn

¹ School of Mechanical Engineering, Tongji University, Shanghai 201804, China

force and edge defects; the influence of the drilling depth on the drilling force was the most remarkable, and the drilling force was closely related to edge defects.

Grinding is an important precision and ultra-precision processing method in manufacturing. Zhong et al. [9] grinded SiCp/Al composite with volume fractions of 10% and 20% using diamond and silicon carbide grinding wheels: they observed that, when using the silicon carbide grinding wheel, the grinded surface was coated with aluminium alloy; on the contrary, when using the diamond grinding wheel, the aluminium alloy did not easily adhere to the surface and a higher surface quality could be obtained. Ronald et al. [10] adopted the resin bonded and electroplated diamond wheel to grind SiCp/Al composite with a volume fraction of 30%. It was found that the resin-bonded diamond grinding wheel was better than the electroplated diamond grinding wheel. Shanawaz et al. [11] studied the electrolytic in-process dressing online dressing technology of SiCp/Al composite with a volume fraction of 10% and found that the normal grinding force curve was periodic and unstable during ELID grinding. As the electrical current increases, the grinding surface roughness and microhardness of SiCp/Al composite increase too. Huang and Yu [12] studied the grinding force of SiCp/Al composite under different grinding conditions: they observed that the grinding force was the highest in low-temperature environments and the lowest in wet environments. Zhou et al. [13] analysed the grinding technique of SiCp/Al composite with a coolant of liquid nitrogen: it was found that liquid nitrogen cooling could improve the support ability of the matrix to silicon carbide particles, and the brittle damage of silicon carbide particles was inhibited, thus grinding surface quality was improved. Zha et al. [14] studied the material removal mechanism of high-volume fraction of SiCp/Al composite by ultrasonic-assisted grinding experiments. They found that the removal mode of particles played a decisive role in the machined surface quality and that appropriate process parameters could effectively improve the final surface quality. Liang et al. [15] proposed a new process technology for ultrasonic-assisted grinding of SiCp/Al composite: the surface quality of the thin-walled workpiece was taken as an evaluation parameter, the effects of grinding direction and ultrasonic action on the surface morphology and quality were studied, and the process performance of ultrasonic-assisted grinding was also explored. Jia et al. [16] investigated the surface topography of NMQL (nanofluid minimum quantity lubrication) grinding ZrO₂ ceramics with ultrasonic vibration and discovered that the adhesion and material peeling phenomenon on the workpiece surface can be evidently reduced compared with that after dry grinding without ultrasonic vibration. Gao et al. [17] developed a kinematic model, the grain and workpiece relative motion

trails in 2D ultrasonic vibration-assisted grinding (UVAG) were simulated at different resultant vibration angles, and they analysed the grain's cutting characteristics and found them conducive to the full infiltration of nanofluids into the grinding zone. Moreover, Yang et al. [18, 19] developed the prediction models of minimum chip thickness and ductile–brittle transition chip thickness during single-diamond grain grinding of zirconia ceramics under dry and different lubricating conditions; the size effect was also considered in the prediction model, and it showed that the predicted values were consistent with the experimental values.

Many researchers have investigated the grinding force prediction models, but few people have applied idea of the big data and machine learning in the grinding process. In this study, the grinding process was regarded as a black box. Single-abrasive-grain grinding experiments were designed, and the respective grinding forces were measured at different grinding process parameters. Subsequently, a prediction model for the single-abrasive-grain grinding force was established to study the influence of the grinding process parameters and grinding grain angle on the grinding force of SiCp/Al composite. Furthermore, multi-abrasive-grain grinding experiments were conducted to measure the forces under different grinding conditions, and the support vector machine (SVM) prediction method (based on particle swarm optimisation (PSO)) was used to establish a prediction model for the multi-abrasive-grain grinding force of SiCp/Al composite.

2 Experimental details

2.1 Materials

The investigated material was SiCp/Al composite (produced by Xi'an Chuangzheng New Materials Company, China), and its matrix was aluminium alloy A356.2 with a volume content of silicon carbide of approximately 70%. The material was produced by pressure die casting; its properties are listed in Table 1.

Table 1 Properties of SiCp/Al composite

Parameter	Value
Thermal conductivity (w/(m k))	226.4
Diffusivity (mm ² /s)	90.105
Density (g/cm ³)	2.97
Heat capacity (J/(g k))	0.846
Elastic modulus (GPa)	190

2.2 Experimental apparatus

2.2.1 Grinding machine

The CNC surface grinder (Schleifring K-P36 Compact, Germany) was used for the experiments. The multi-abrasive grinding wheel was an electroplated diamond grinding wheel with a diameter of 300 mm, thickness of 30 mm, grain size of 120 mesh, and concentration of 100%; thus, the abrasive layer had 0.88 g synthetic diamond per square centimetre on average [20, 21]. The abrasive-grain angle on the grinding wheel ranged from approximately 90° to 135°.

2.2.2 Single-abrasive-grain grinding system

A single-abrasive grinding wheel was adopted to process the SiCp/Al composite; its section diagram is shown in Fig. 1. The diameter and thickness of the grinding wheel (made from aluminium alloy) were 300 and 30 mm, respectively.

The material of the single-abrasive grain on the grinding wheel was diamond, such as for the abrasive grinding wheel used in the multi-abrasive-grain grinding experiments. To keep the grinding wheel balanced during rotation, the counterweight balance screw was made of the same material as the pillar. The cylindrical diamond pillar and counterweight balance screw were inserted into the grinding wheel, and the grinding wheel was assembled on the grinding machine spindle.

Moreover, two M10 threaded holes were symmetrically created in the upper and lower parts of the grinding wheel, and the cylindrical pillar with diamond top was tapped with a

thread and assembled radially on the side of the single-abrasive grinding wheel. In the grinding process, the ration of the normal and tangential grinding forces was between 1.2 and 2.5; therefore, the angles of the abrasive diamond grain were set to 90°, 105°, 120°, and 135°, respectively.

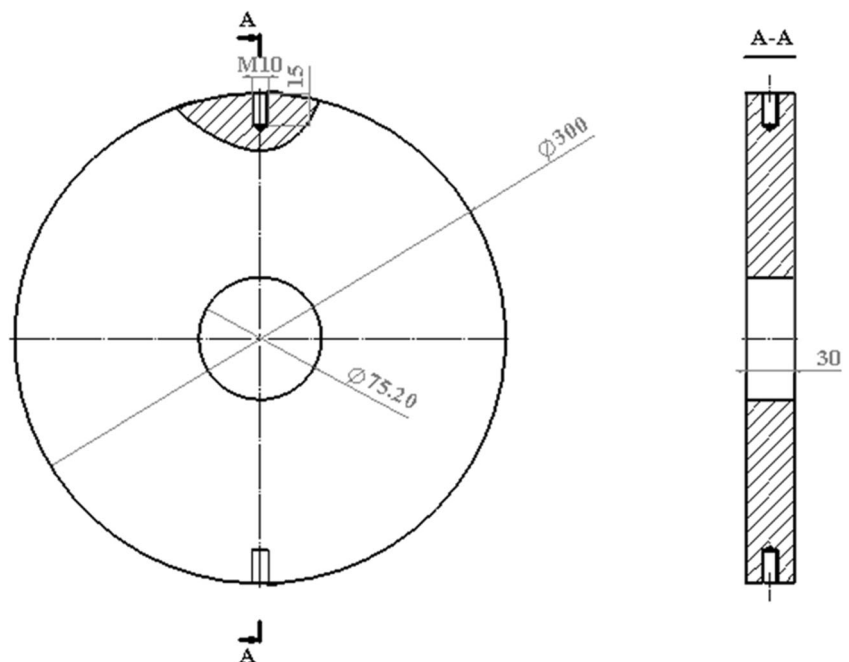
Figure 2 shows the single-abrasive-grain grinding system for SiCp/Al composite: it consisted of a fixture, a force sensor, a signal condition device, an A/D conversion device, and a computer. The fixture, force sensor, and base were connected by screws to guarantee meshing strength. The grinding force was measured using the strain gauge, which transmitted the value to the signal conditioning device and then the A/D conversion device; finally, the signal was processed by the computer. The data acquisition frequency of the grinding force sensor was 512 Hz.

2.3 Experimental process

In the single-abrasive-grain grinding process with SiCp/Al composite, the single-abrasive-diamond grain grinding wheel rotated at the speed v_s , the feed velocity was v_w , and the grinding depth was a_p . The force sensor recorded the grinding force throughout the experimental process; the recorded force was then transferred to the computer via an RS485 protocol and was analysed using LabVIEW.

Figure 3 shows the grinding force of single-abrasive-grain grinding of SiCp/Al composite when the abrasive-grain angle is 90°. The normal and tangential forces are approximately equal. When the abrasive grain contacts the workpiece, the grinding force increases, and when the abrasive diamond grain moves away from the SiCp/Al composite workpiece, the

Fig. 1 Single-abrasive grinding wheel



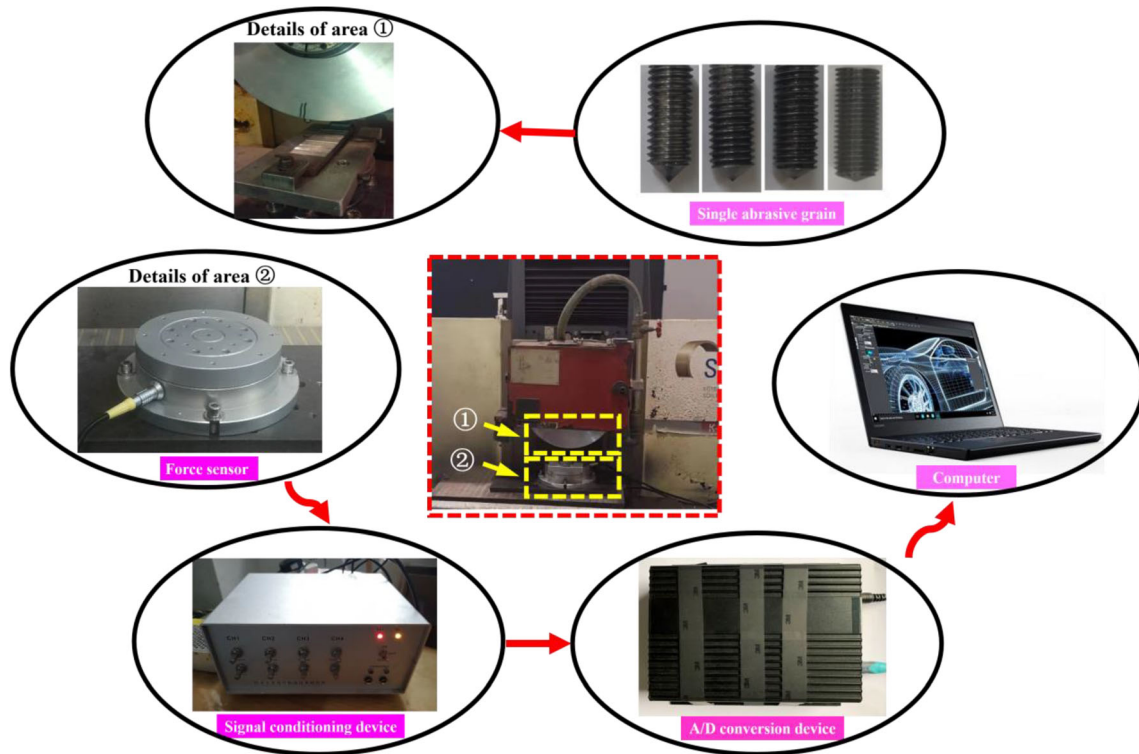


Fig. 2 Single-abrasive-grain grinding system for SiCp/Al composite

grinding force decreases gradually to zero. In this grinding process, the grinding wheel contacts the workpiece every cycle; therefore, the grinding signal exhibits fluctuations.

2.4 Experiment design

According to the requirements of central composite design, a three-factor and three-level experimental schedule

was developed; x_1 is the wheel speed v_s , x_2 the feed velocity v_w , and x_3 the grinding depth a_p . The wheel speed v_s ranges from 10 to 30 m/s, the grinding depth a_p from 0.05 to 0.15 mm, and the feed velocity v_w from 0.3 to 0.9 m/min. In addition, s_1 , s_0 , and s_{-1} represent the 1, 0, and -1 levels of each processing variable:

$$x_i = \frac{s_i - s_{0i}}{\Delta_i}, i = 1, 2, 3,$$

where x_i is the variable code, s_i the processing variable parameter, s_{0i} the level zero of the grinding parameter variable, and Δ_i the variation interval of the current parameters. The coding table of the grinding processing parameters is shown in Table 2.

A total of 15 groups of experiments were designed according to the principles of the central composite surface design (central composite face-centred; CCF), which is an

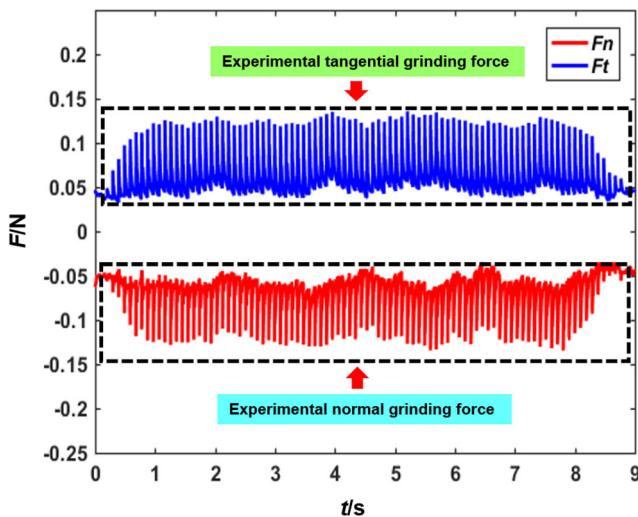


Fig. 3 Single-abrasive-grain grinding force of SiCp/Al composite

Table 2 Coding table of grinding processing parameters

Effect	Parameter and unit	Level		
		- 1	0	1
A	v_s (m/s)	10	20	30
B	v_w (m/min)	0.3	0.6	0.9
C	a_p (mm)	0.05	0.1	0.15

Table 3 Grinding processing parameters of SiCp/Al composite

No.	v_s (m/s)	v_w (m/min)	a_p (mm)	x_1	x_2	x_3
1	10	0.9	0.15	-1	1	1
2	10	0.3	0.15	-1	-1	1
3	10	0.9	0.05	-1	1	-1
4	10	0.3	0.05	-1	-1	-1
5	10	0.6	0.1	-1	0	0
6	30	0.3	0.15	1	-1	1
7	30	0.9	0.15	1	1	1
8	30	0.6	0.1	1	0	0
9	30	0.9	0.05	1	1	-1
10	30	0.3	0.05	0	-1	-1
11	20	0.6	0.15	0	0	1
12	20	0.3	0.1	0	-1	0
13	20	0.9	0.1	0	1	0
14	20	0.6	0.05	0	0	-1
15	20	0.6	0.1	0	0	0

experimental orthogonal-response design method. The results are listed in Table 3.

3 Grinding force prediction model for SiCp/Al composite

Figure 4 illustrates the technique route of the grinding force prediction model for SiCp/Al composite. The single-abrasive-grain grinding experiments were designed, and the grinding forces were measured considering different grinding process parameters. Subsequently, a prediction model for the single-abrasive-grain grinding force was established to study the influence of the grinding process parameters and grain angles on

the grinding force of SiCp/Al composite. In addition, multi-abrasive-grain grinding experiments were conducted under different grinding conditions, and the resulting forces were measured. The SVM prediction method based on PSO was used to establish a multi-abrasive-grain grinding force prediction model for SiCp/Al composite.

3.1 Theoretical prediction model for single-abrasive-grain grinding force of SiCp/Al composite

3.1.1 Equivalent grinding depth

The thickness of the undeformed grinding chips is random in the grinding process, and the probability density function can be adopted to calculate it (Fig. 5). According to the literature review, the thicknesses of the undeformed grinding chips in the contact area can be assumed to obey the Rayleigh distribution [22]:

$$f(h) = \begin{cases} \left(\frac{h}{m^2}\right)e^{-(h^2/2m^2)}, & h \geq 0 \\ 0, & h < 0 \end{cases} \quad (1)$$

where $E(h) = \sqrt{\frac{\pi}{2}}m$ and $\sigma(h) = \sqrt{\frac{4-\pi}{2}}m$.

The number of abrasive grains per unit area N_s can be determined with a microscope, and the contact arc length between the grinding wheel and workpiece l_a in Fig. 6 can be expressed as follows:

$$l_a = R \cdot \arccos \frac{R-a_p}{R} \quad (2)$$

The total number N_{total} of particles in the grinding area per unit time is as follows:

$$N_{total} = v_s b N_s \quad (3)$$

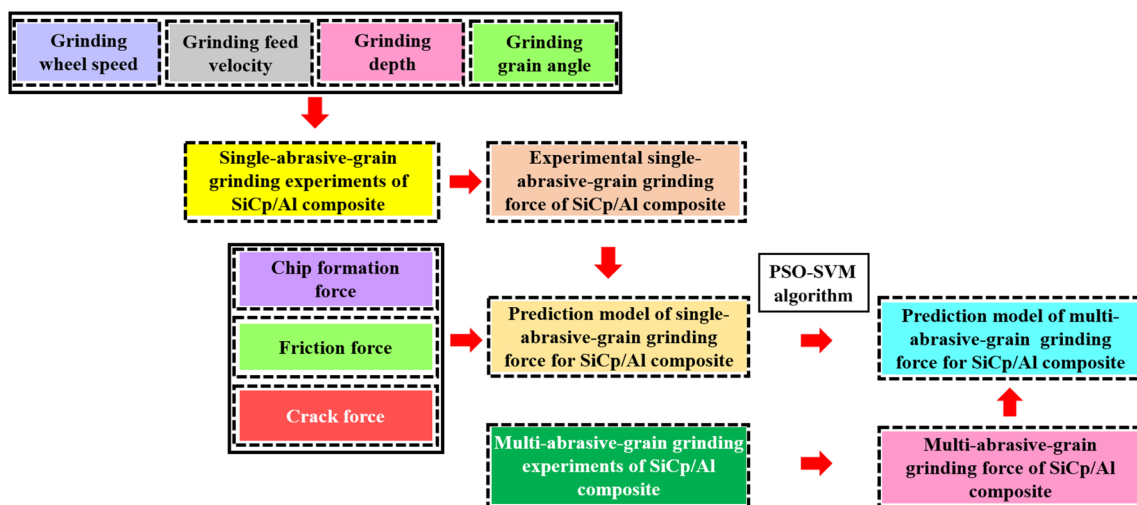


Fig. 4 Technique route of grinding force prediction model of SiCp/Al composite

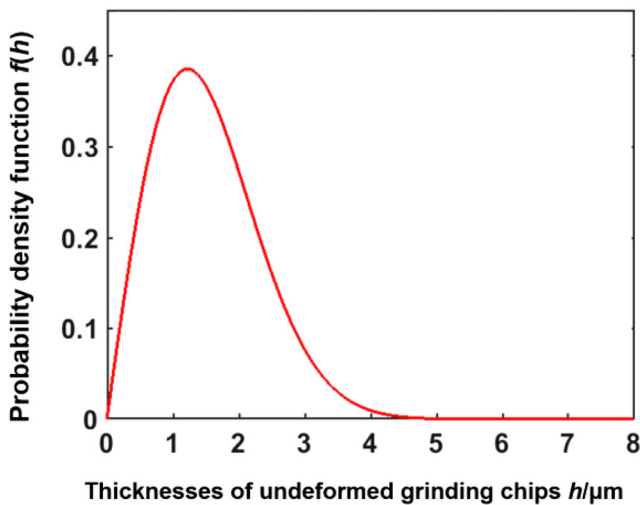


Fig. 5 Chip thickness probability density function curve

and the cross-sectional area $E(A)$ of the undeformed chip can be expressed as follows:

$$E(A) = E(h^2) \tan\theta. \tag{4}$$

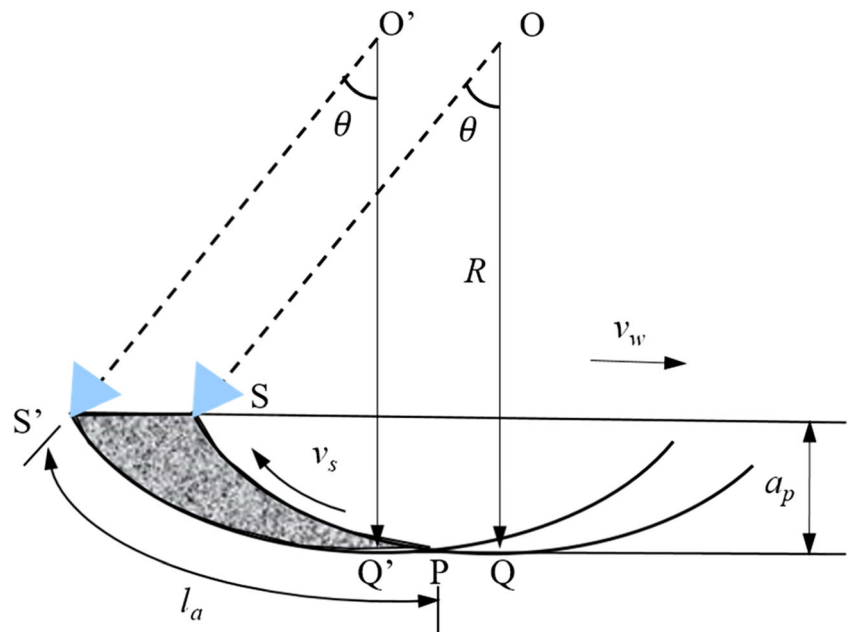
The volume V_c of the undeformed chip is presented in Eq. 5:

$$V_c = E(h^2) \tan\theta l_a. \tag{5}$$

The grinding process can be regarded as an abrasive manufacturing process with a rotating grinding wheel and a workpiece feeding system below a certain grinding depth. In 1 s, the removal rate V of the grinded material is:

$$V = ba_p v_w. \tag{6}$$

Fig. 6 Schematic of motion trajectory of abrasive grain



Assuming uniform abrasive removal, the material removal rate V can be expressed as follows:

$$V = v_s N_s E(A) b l_a, \tag{7}$$

$$E(A) = \frac{a_p v_w}{N_s v_s l_a}, \tag{8}$$

$$E(h^2) = \frac{a_p v_w}{N_s v_s l_a \tan\theta}. \tag{9}$$

Therefore, the equivalent grinding depth of the abrasive grains is expressed as follows:

$$E(h) = \sqrt{E(h^2)} \cdot \frac{\sqrt{\pi}}{2} = \sqrt{\frac{\pi a_p v_w}{4 N_s v_s l_a \tan\theta}}. \tag{10}$$

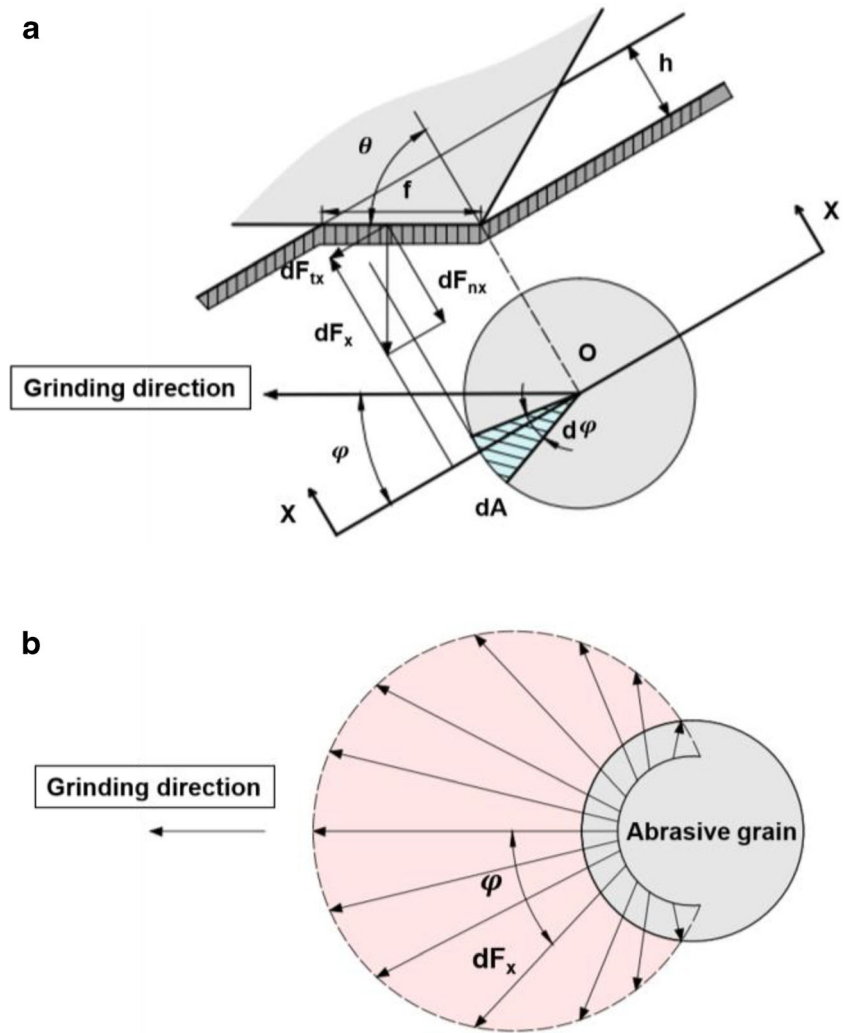
3.1.2 Single-abrasive-grain grinding force of SiCp/Al composite

The grinding force of the SiCp/Al composite is mainly composed of chip formation, friction, and cracking forces of the silicon carbide. Therefore, the overall grinding force can be expressed as follows:

$$\begin{cases} F_{gt} = F_{ct} + F_{ft} + F_{rt} \\ F_{gn} = F_{cn} + F_{fn} + F_{rn} \end{cases}, \tag{11}$$

where F_{gt} is the total tangential force, F_{gn} the total normal force, F_{ct} the chip formation tangential force, F_{cn} the chip formation normal force, F_{fn} the friction tangential force, F_{fn} the friction normal force, F_{rt} the cracking tangential force, and F_{rn} the cracking normal force.

Fig. 7 Schematic diagram of single-abrasive-grain grinding. **a** Section diagram of single-abrasive-grain grinding. **b** Top view of single-abrasive-grain grinding



Prediction model for chip formation force of SiCp/Al composite Figure 7 presents a schematic of the grinding process: a single-abrasive grain grinds the workpiece, and the pressure along the surface is not constant. The grinding force can be calculated with integration equations [23].

The grinding force dF_x acting on the abrasive grains of the $X-X$ section is:

$$dF_x = F_p dA \cos\theta \cos\psi, \tag{12}$$

where F_p is the unit grinding force, dA the contact area of the grinding wheel, θ the semi-top angle of the abrasive grain, and ψ the angle between the grinding force direction and x direction.

The contact area is as follows:

$$dA = \frac{1}{2} \rho^2 \sin^2\theta d\psi, \tag{13}$$

and the grinding force dF_x can be expressed as follows:

$$dF_x = \frac{1}{2} \rho^2 F_p \sin\theta \cos\theta \cos\psi d\psi. \tag{14}$$

Owing to the following expression

$$\begin{cases} dF_t = dF_x \cos\theta \\ dF_n = dF_x \sin\theta \end{cases}, \tag{15}$$

the grinding forces dF_x and dF_n can be expressed as follows:

$$\begin{cases} dF_t = \frac{1}{2} \rho^2 F_p \sin\theta \cos^2\theta \cos\psi d\psi \\ dF_n = \frac{1}{2} \rho^2 F_p \sin^2\theta \cos\theta \cos\psi d\psi \end{cases}. \tag{16}$$

The grinding forces acting on the single-abrasive grain are as follows:

$$\begin{cases} F_{ct} = \int_{-\frac{\pi}{2}}^{\frac{\pi}{2}} \frac{dF_t}{d\psi} d\psi = \frac{\pi}{4} \rho^2 F_p \sin\theta \cos^2\theta = \frac{\pi}{4} h^2 F_p \sin\theta \\ F_{cn} = \int_{-\frac{\pi}{2}}^{\frac{\pi}{2}} \frac{dF_n}{d\psi} d\psi = \rho^2 F_p \sin\theta \cos^2\theta = F_p h^2 \sin\theta \tan\theta \end{cases}, \tag{17}$$

where h represents the average chip thickness. Thus, the grinding force acting on the single-abrasive grain can be written as follows:

$$\begin{cases} F_{ct} = \frac{\pi}{4} \frac{F_p a_p v_w}{N_s v_s l_a} \cos\theta = C_1 \frac{a_p v_w}{N_s v_s l_a} \cos\theta \\ F_{cn} = \frac{F_p a_p v_w}{N_s v_s l_a} \sin\theta = C_1 \frac{4}{\pi} \frac{a_p v_w}{N_s v_s l_a} \sin\theta \end{cases}. \tag{18}$$

Where C_1 is a constant because different abrasive angles may cause different working contact conditions, the coefficients k_1 and k_2 were adopted to modify the chip formation force:

$$\begin{cases} F_{ct} = k_1 \frac{a_p v_w}{N_s v_s l_a} \\ F_{cn} = k_2 \frac{a_p v_w}{N_s v_s l_a} \end{cases}. \tag{19}$$

Friction force prediction model for SiCp/Al composite

According to the grinding principle:

$$\begin{cases} F_{ft} = \mu \delta \Delta p \\ F_{fn} = \delta \Delta p \end{cases}, \tag{20}$$

where Δp is the pressure between the contact surface and sample surface, and μ is the friction coefficient between the abrasive grain and workpiece. In the high-speed grinding experiment, the friction coefficient μ can be determined by fitting the measured grinding force.

The average pressure p between the contact and workpiece surfaces is presented based on [23]:

$$p = p_0 V = \frac{4p_0 v_w}{d_s v_s}, \tag{21}$$

where p_0 is a constant that can be determined by fitting the experimental results.

The friction force components can be expressed as follows:

$$\begin{cases} F_{ft} = 4\pi a_p^2 p_0 v_w \tan\theta \mu / (d_s v_s) \\ F_{fn} = 4\pi a_p^2 p_0 v_w \tan\theta / (d_s v_s) \end{cases}. \tag{22}$$

Because different abrasive angles may cause different friction conditions, the coefficients k_3 and k_4 are adopted to modify the friction force:

$$\begin{cases} k_3 = 4\pi p_0 \mu \\ k_4 = 4\pi p_0 \end{cases}.$$

Consequently, the friction force can be expressed as follows:

$$\begin{cases} F_{ft} = k_3 a_p^2 v_w / (d_s v_s) \\ F_{fn} = k_4 a_p^2 v_w / (d_s v_s) \end{cases}. \tag{23}$$

Cracking force prediction model for SiCp/Al composite

In the grinding process of SiCp/Al composite, the silicon carbide is sheared by the abrasive grain. As a result, horizontal and vertical cracks can easily occur, and the silicon carbide can easily break into pieces; thus, the cracking force of silicon carbide should be considered [24, 25].

According to Griffith’s theory, the change in the potential energy caused by the debonding damage is related to the volume fraction of silicon carbide and its material properties [26]:

$$G = \frac{dU}{dS} = \frac{K^2(1-\nu^2)}{E}, \tag{24}$$

$$K^2 = \pi \sigma^2 l, \tag{25}$$

$$dS = w dl, \tag{26}$$

$$\sigma = \frac{K_{IC}}{\sqrt{d}}, \tag{27}$$

where U is the strain energy, S the interface crack area, K the stress intensity, E the elastic modulus, ν Poisson’s ratio, l the interface crack length, w the initial interface crack width, K_{IC} the fracture toughness, and d the size of the silicon carbide particles.

The initial length l_i of the interface crack and initial width w of the interface crack are assumed to be 1 μm ; thus, the strain energy consumed for fracture can be expressed as follows:

$$U = \int_{l_i}^{l_f} \frac{\pi w K_{IC}^2 (1-\nu^2)}{Ed} dl. \tag{28}$$

The fracture fraction of silicon carbide is equal to the volume fraction [27, 28], and the number of fractured or debonding silicon carbide particles can be expressed as follows:

$$n_f = \frac{1}{\frac{4}{3} \pi \left(\frac{d}{2}\right)^3 v_d^2}, \tag{29}$$

where v_d is the volume fraction of silicon carbide.

According to the energy conservation law, the relationship between the fracture force and strain energy consumed for fracture can be expressed as follows:

$$F_f = n_f U b a_p \tag{30}$$

Because different abrasive angles may cause different strain energies, the coefficients k_5 and k_6 are adopted to modify the fracture force:

$$\begin{cases} F_{kt} = k_5 b a_p \\ F_{kn} = k_6 b a_p \end{cases} \tag{31}$$

3.1.3 Prediction model for single-abrasive-grain grinding force of SiCp/Al composite

The single-abrasive-grain grinding force of SiCp/Al composite consists of the chip formation force, the friction force, and the cracking force, and different abrasive grain angles may have different effects on the grinding force.

Based on the chip formation force, the friction force, and the cracking force prediction model of SiCp/Al composite, the single-abrasive-grain grinding force prediction model for SiCp/Al composite can be formulated as:

$$\begin{cases} F_{gt} = k_1 \frac{a_p v_w}{N_s v_s l_a} + k_3 a_p^2 v_w / (d_s v_s) + k_5 b a_p \\ F_{gn} = k_2 \frac{a_p v_w}{N_s v_s l_a} + k_4 a_p^2 v_w / (d_s v_s) + k_6 b a_p \end{cases} \tag{32}$$

Subsequently, the least squares method is adopted to determine the best parameters. After fitting, the prediction model for the single-abrasive-grain grinding force (angle of 90°) of the SiCp/Al composite can be expressed as follows:

$$\begin{cases} F_{gt} = 1.959 \times 10^2 \frac{a_p v_w}{N_s v_s l_a} + 1.398 \times 10^5 a_p^2 v_w / (d_s v_s) + 0.207 b a_p \\ F_{gn} = 2.092 \times 10^2 \frac{a_p v_w}{N_s v_s l_a} + 2.263 \times 10^5 a_p^2 v_w / (d_s v_s) + 0.193 b a_p \end{cases} \tag{33}$$

The prediction model for the single-abrasive-grain grinding force (angle of 105°) of the SiCp/Al composite can be written as follows:

$$\begin{cases} F_{gt} = 1.671 \times 10^2 \frac{a_p v_w}{N_s v_s l_a} + 2.289 \times 10^5 a_p^2 v_w / (d_s v_s) + 0.309 b a_p \\ F_{gn} = 2.239 \times 10^2 \frac{a_p v_w}{N_s v_s l_a} + 3.759 \times 10^5 a_p^2 v_w / (d_s v_s) + 0.343 b a_p \end{cases} \tag{34}$$

Moreover, that of the single-abrasive-grain grinding force at a grain angle of 120° can be expressed as follows:

$$\begin{cases} F_{gt} = 2.463 \times 10^2 \frac{a_p v_w}{N_s v_s l_a} + 2.799 \times 10^5 a_p^2 v_w / (d_s v_s) + 0.322 b a_p \\ F_{gn} = 3.067 \times 10^2 \frac{a_p v_w}{N_s v_s l_a} + 4.378 \times 10^5 a_p^2 v_w / (d_s v_s) + 0.551 b a_p \end{cases} \tag{35}$$

and that of the single-abrasive-grain grinding force at a grain angle of 135° can be expressed as follows:

$$\begin{cases} F_{gt} = 2.815 \times 10^2 \frac{a_p v_w}{N_s v_s l_a} + 2.834 \times 10^5 a_p^2 v_w / (d_s v_s) + 0.384 b a_p \\ F_{gn} = 4.137 \times 10^2 \frac{a_p v_w}{N_s v_s l_a} + 4.672 \times 10^5 a_p^2 v_w / (d_s v_s) + 0.561 b a_p \end{cases} \tag{36}$$

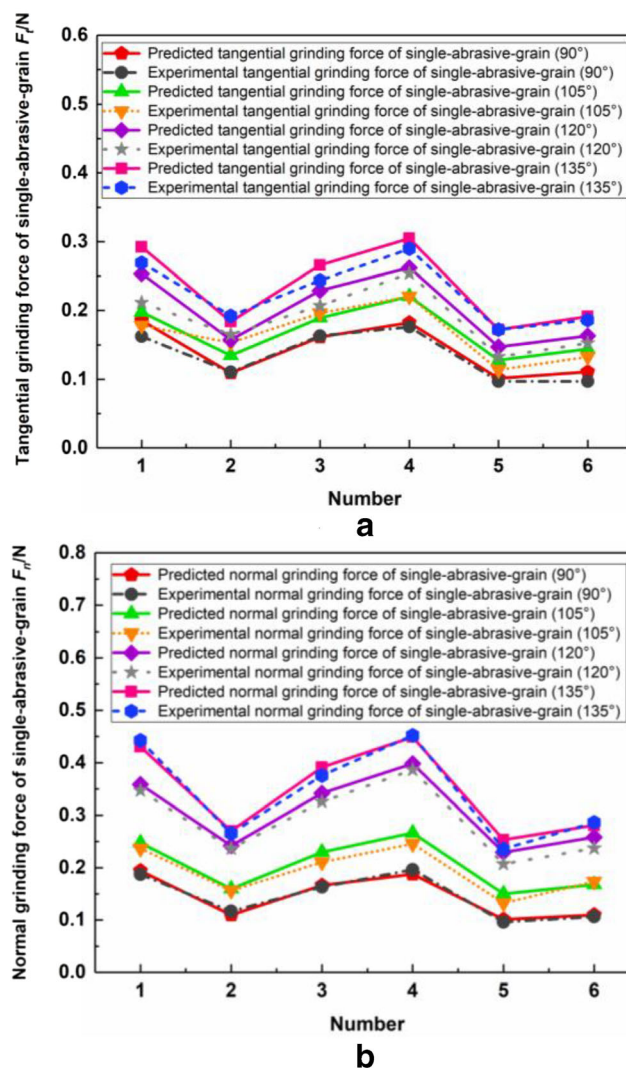


Fig. 8 Comparison of predicted and experimental grinding forces of single-abrasive grain. a Tangential grinding force. b Normal grinding force

3.1.4 Evaluation of prediction model for single-abrasive-grain grinding force of SiCp/Al composite

Six experiments were conducted to verify the theoretical prediction model for the single-abrasive-grain grinding force of SiCp/Al composite. Figure 8 compares the predicted and experimental grinding forces; evidently, the predicted single-abrasive-grain tangential and normal grinding forces are in good agreement with the experimental results. Therefore, the theoretical prediction model can be applied to predict the single-abrasive-grain grinding force of SiCp/Al composite.

3.2 Grinding force prediction model for SiCp/Al composite

As demonstrated in Fig. 9, in the traditional grinding force prediction model, the wheel speed, feed velocity, and grinding depth are the input parameters. In this study, the grinding process was regarded as a black box with many grinding factors such as the dynamic effect and abrasive-grain distribution in the grinding process; the output is the grinding force.

Moreover, the abrasive-grain angle was removed and considered from the grinding black box. Figure 10 presents the grinding force prediction model based on single-abrasive-grain grinding. Based on the total grinding force of the SiCp/Al composite, the average single-abrasive-grain grinding force can be calculated. In addition, based on the single-abrasive-grain grinding experiments, the grinding forces of the abrasive grain with angles of 90°, 105°, 120°, and 135° can be determined. The resulting grinding force has a nonlinear relationship with the experimental average grinding force of the single-abrasive grain. The SVM prediction method based on PSO can establish a nonlinear mathematic model, which can be used to create a grinding force prediction model for the SiCp/Al composite.

3.2.1 Particle swarm optimisation algorithm

PSO is an evolutionary computational algorithm based on the behavioural study of bird predation. Its basic idea is finding the optimal solution through the cooperation and information sharing among individuals in the group.

Figure 11 shows how the PSO algorithm works. When an optimisation problem is regarded as a foraging bird flock in PSO, food is the optimal solution in the problem, and every foraging bird flying in the air is a searching particle in the solution space of the PSO algorithm.

For a search in an N -dimensional space, the information of the i th particle can be represented by a two-dimensional vector.

The position of the i th particle can be expressed as follows:

$$x_i = (x_{i1}, x_{i2}, \dots, x_{iN})^T,$$

and its speed is as follows:

$$v_i = (v_{i1}, v_{i2}, \dots, v_{iN})^T.$$

After finding the two optimal solutions, the particles can update their speed and position according to the following relations:

$$v_{id}^{k+1} = v_{id}^k + c_1 \times rand_1^k \times (Pbest_{id}^k - x_{id}^k) + c_2 \times rand_2^k \times (Gbest_{id}^k - x_{id}^k), \tag{37}$$

$$x_{id}^{k+1} = x_{id}^k + v_{id}^{k+1}, \tag{38}$$

where v_{id}^{k+1} is the velocity of the i th particle in the d th dimension at the k th iteration, and x_{id}^{k+1} is the position of the i th particle in the d th dimension at the k th iteration; if the values of the c_1 and c_2 learning factors are feasible, they can accelerate convergence and prevent the PSO from falling into a local optimum; moreover, $Pbest_{id}^k$ is the position of the i th particle at the individual extreme point of the d th dimension, and

Fig. 9 Schematic diagram of traditional grinding force prediction model

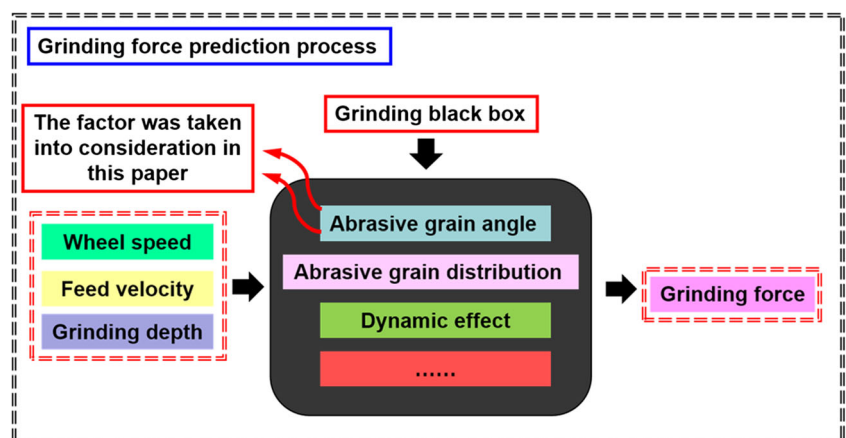
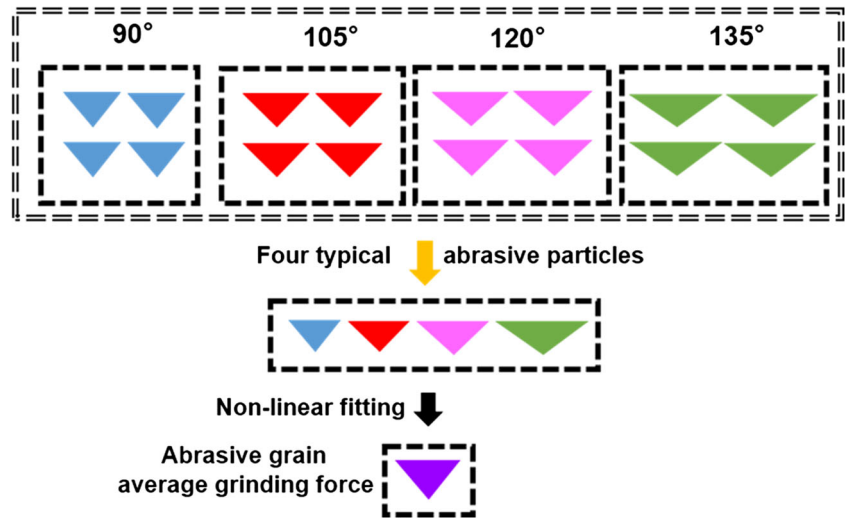


Fig. 10 Schematic diagram of grinding force prediction model based on single-abrasive-grain grinding



$Gbest_{id}^k$ is the position of the entire population at the global extreme point of the d th dimension.

When the number of reiterations is below the set maximum, the particle velocity and position are continuously updated to determine the corresponding fitness value. When the number of iterations reaches the set maximum, the optimal fitness value is reached: the corresponding particle velocity and position are the output and considered the optimal solution.

3.2.2 Support vector machine algorithm

The SVM algorithm is based on statistical learning. By constructing the optimal hyperplane, the classification error for unknown samples is consequently minimised. According to structural risk minimisation, the SVM minimises the VC confidence by constructing optimal hyperplanes under the conditions of a fixed learning experience risk [29] (Fig. 12).

Moreover, each set of experimental parameters constitutes a sample dataset $\{x(i), F_i\}_{i=1}^n$; the prediction model can be

expressed as follows:

$$y(x) = y_F(x) = w^T \varphi(x) + b, \tag{39}$$

where w^T is a vector, $\varphi(x)$ a high-dimensional space vector obtained by the nonlinear mapping of the vector x , and $y(x)$ a hyperplane; the deviation b can be determined as follows:

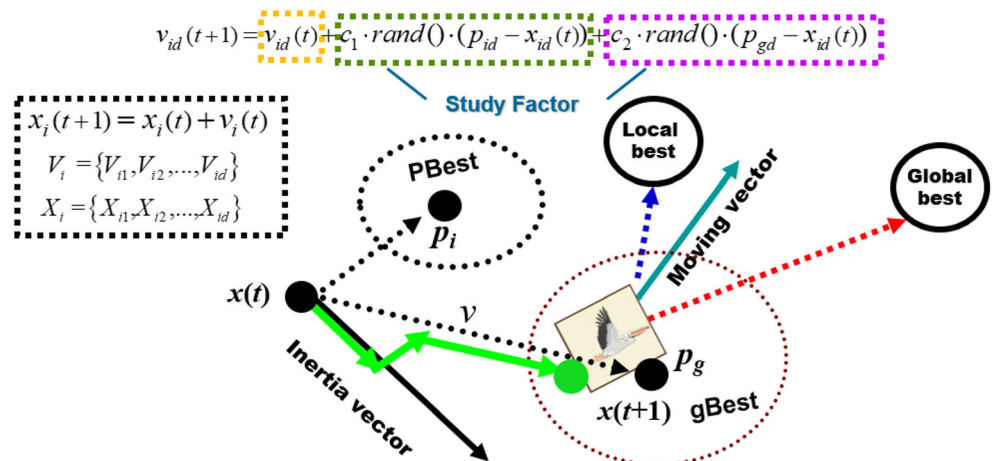
$$\min R(y) = \min \left(\|w\|^2 + \mu \frac{1}{2} \sum_{i=1}^n L(y_i, y_F) \right) \tag{40}$$

where $L(y_i, y_{Ra})$ is the loss function and μ the penalty coefficient, which are mainly used to balance the training errors and model complexity. To ensure high accuracy of the SVM-based prediction model, a small positive number ε is introduced:

$$|y_i - y(x)| = |F_i - y_F(x)| \leq \varepsilon \tag{41}$$

For the hyperplane, finding the optimal solution means that the splitting gap is maximal. The slack variables ξ and ξ^* are

Fig. 11 Schematic diagram of PSO algorithm



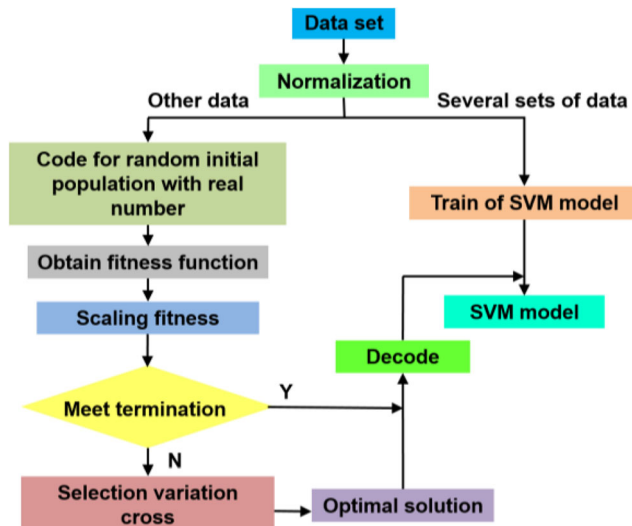


Fig. 12 Scheme diagram of SVM optimisation process

introduced to ensure that the problem has a solution. The computation process of the optimal solution is as follows:

$$\min R(w, b) = \min \left(\frac{1}{2} \|w\|^2 + \frac{1}{2} \mu \sum_{i=1}^n (\xi_i + \xi_i^*) \right), \quad (42)$$

$$s.t. \quad \begin{aligned} w^T \varphi(x) + b - y_i &\leq \varepsilon + \xi_i \\ y_i - w^T \varphi(x) - b &\leq \varepsilon + \xi_i^* \\ \xi_i, \xi_i^* &\geq 0 \\ i &= 1, 2, \dots, n \end{aligned}$$

which represents a quadratic programming problem. Therefore, a Lagrange operator is introduced:

$$L = \frac{1}{2} \|w\|^2 + \frac{1}{2} \mu \sum_{i=1}^n (\xi_i + \xi_i^*) - \sum_{i=1}^n \lambda_i (\varepsilon + \xi_i - w^T \varphi(x) - b + y_i) - \sum_{i=1}^n \lambda_i^* (\varepsilon + \xi_i^* + w^T \varphi(x) + b - y_i). \quad (43)$$

where λ_i and λ_i^* are Lagrange multipliers. Under the KKT condition, Eq. 41 can be transformed into a dual optimisation problem:

$$\min \quad \frac{1}{2} \sum_{i=1}^n \sum_{j=1}^n (\lambda_i - \lambda_i^*) (\lambda_j - \lambda_j^*) k(x_i, x_j) + \varepsilon \sum_{i=1}^n (\lambda_i + \lambda_i^*) - \sum_{i=1}^n y_i (\lambda_i - \lambda_i^*). \quad (44)$$

$$s.t. \quad \sum_{i=1}^n (\lambda_i - \lambda_i^*) = 0,$$

$$0 \leq \lambda_1, \lambda_1^* \leq \mu.$$

According to Mercer's condition:

$$k(x_i, x_j) = \varphi^T(x_i) \cdot \varphi(x_j), \quad (45)$$

where $k(x_i, x_j)$ is the kernel function. Because the grinding

process of SiCp/Al composite exhibits significant nonlinearities, the radial basis kernel function is more suitable for this case.

The Gaussian kernel function is presented below with g as the width:

$$k(x_i, x_j) = \exp \left(-g \|x_i - x_j\|^2 \right). \quad (46)$$

Then, tangential and normal grinding force prediction models for the SiCp/Al composite can be deduced using the same method. They are defined as follows:

$$y_{Fi}(x) = \sum_{i=1}^n (\lambda_{1i} - \lambda_{1i}^*) k_1(x_i, x_j) + b_1, \quad (47)$$

$$y_{Fn}(x) = \sum_{i=1}^n (\lambda_{2i} - \lambda_{2i}^*) k_2(x_i, x_j) + b_2. \quad (48)$$

3.2.3 Support vector machine prediction model based on particle swarm optimisation algorithm

The PSO algorithm was chosen to optimise the kernel function width g , punishment factor μ , and sensitivity coefficient ε . The initial value was randomly chosen, and the maximal hereditary algebra was set to 200. Moreover, the mean-squared error between the prediction and experimental values was adopted as the fitness value; the fitness function $E(f)$ can be expressed as follows:

$$E(f) = \sum_{i=1}^n |y_i - y_F(x)| \quad (49)$$

The main steps in the algorithm flow of the PSO–SVM prediction model are as follows:

- (1) The grinding process parameters of the SiCp/Al composite are normalised and inserted into the model for training.
- (2) Once the initial velocity and position of the particle swarm are set, the width g , penalty factor μ , and sensitivity coefficient ε are determined for each iteration, and the PSO algorithm is improved.
- (3) The iterated kernel width g , penalty factor μ , and sensitivity coefficient ε are substituted into the training data of the vector machine, and the predicted value is obtained. The variance between the prediction and expected values is used as the individual fitness value.
- (4) When the number of iterations does not exceed the maximum, the velocity and position of each particle are iterated to generate a new kernel function width g , penalty factor μ , and sensitivity coefficient ε , and the procedure is continued to train the SVM model.
- (5) Steps (3) and (4) are repeated until the maximal hereditary algebra is reached; the results are the optimal g , μ , and ε .

3.2.4 Grinding force prediction model for SiCp/Al composite

In the actual grinding process, the wheel speed, feed velocity, and grinding depth are determined, and the abrasive grain action during grinding is random. In this study, triangular abrasive grains with angles of 90°, 105°, 120°, and 135° were used. Based on the four predicted abrasive-grain grinding forces at the same grinding process parameters, the prediction model for the single-abrasive-grain grinding force was established.

In the single-abrasive-grain grinding experiments, the grinding depth was set to 0.05–0.15 mm to obtain a more accurate grinding force. In the multi-abrasive-grain grinding experiments, the grinding depth was usually between 0.005 and 0.015 mm, and the single-abrasive-grain grinding force was calculated with the prediction model. Thus, the four predicted abrasive-grain grinding forces can be interpreted as feature recognition vectors, and the average experimental grinding force can be calculated by dividing the multi-abrasive-grain grinding force by the total number of abrasive grains (result is used as output vector). Moreover, the SVM prediction model based on the kernel function was used to predict the multi-abrasive-grain grinding forces at different grinding process parameters. The main technique route is shown in Fig. 13.

The grinding wheel can be modelled as a set of abrasive grains with different properties. Therefore, four triangular abrasive grains with different angles were considered, and the obtained corresponding sets of grinding forces were used as feature recognition vectors to synthesise the multi-abrasive particles.

The traditional process parameters are the wheel speed, feed velocity, and grinding depth, which have limitations regarding the prediction of the grinding force. In this study, abrasive grain angle was

considered. By integrating all factors, four sets of grinding force recognition vectors can be obtained, and the multi-abrasive-grain grinding force can be predicted.

Owing to the large number of random factors in the cutting processes, the grinding forces are considerably affected by the grinding grain angles. Therefore, grinding can be regarded as training a black box with many experiments: the forces measured at different single-grinding grain angles are used as input to predict the total grinding force in the overall contact area. This method ensures better prediction precision than the traditional grinding four-factor prediction model.

In the SiCp/Al composite grinding process, the wheel speeds were 10, 17.5, 25, and 32.5 m/s; the feed velocities were 0.3, 0.6, and 0.9 m/min; the grinding depths were 5, 10, 15, and 20 μm; and the shapes of the abrasive grains were triangular with angles of 90°, 105°, 120°, and 135°. Table 4 shows the predicted force of single-abrasive-grain grinding for different grinding process parameters based on Eqs. 33–36.

After the grinding experiments of the SiCp/Al composite, the number of abrasive grains was calculated, and the grinding forces of the SiCp/Al composite at different process parameters were obtained. The resulting average single-abrasive-grain grinding forces are listed in Table 5.

Figure 14 illustrates the convergence iteration diagram of the PSO algorithm-based SVM, and the deviation prediction for the test group data is shown in Fig. 14. The residual error converges in the 249th and 800th steps of the calculation. Once the iterative process is completed, the optimal parameters of the tangential grinding force prediction model with single-abrasive grain can be determined:

$$g_1 = 0.386, \mu_1 = 199.97, \varepsilon_1 = 0.01.$$

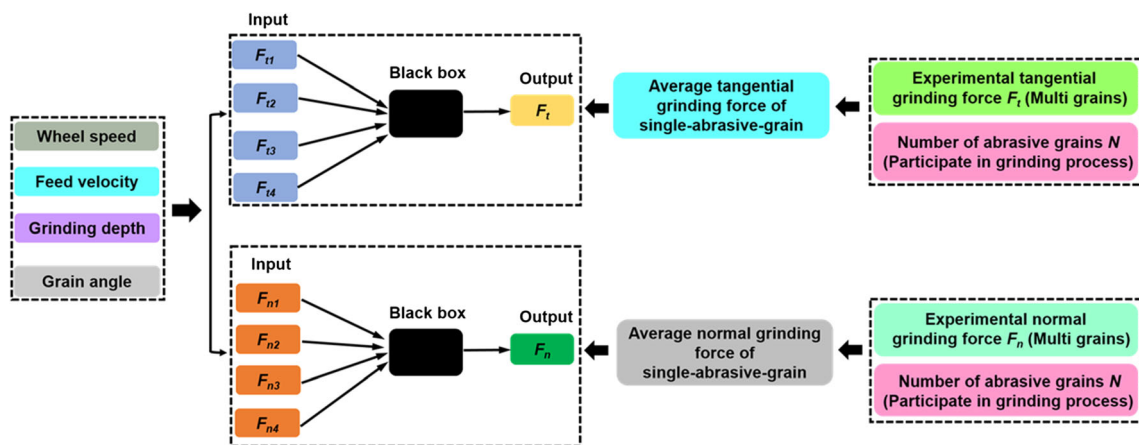


Fig. 13 Details of grinding force prediction model for SiCp/Al composite based on SVM–PSO algorithm

Table 4 Single-grain grinding force of SiCp/Al composite at different grinding process parameters

No.	v_s (m/s)	v_w (m/min)	a_p (μm)	Grain angle	Single grain F_t (N)	Single grain F_n (N)
1	10	0.3	5	90	0.014	0.016
2	10	0.3	5	105	0.017	0.020
3	10	0.3	5	120	0.021	0.028
4	10	0.3	5	135	0.024	0.035
5	10	0.3	10	90	0.022	0.025
6	10	0.3	10	105	0.025	0.031
7	10	0.3	10	120	0.032	0.045
8	10	0.3	10	135	0.037	0.055
...
113	25	0.6	10	90	0.020	0.021
114	25	0.6	10	105	0.022	0.027
115	25	0.6	10	120	0.028	0.039
116	25	0.6	10	135	0.032	0.047
117	25	0.6	15	90	0.027	0.027
118	25	0.6	15	105	0.029	0.035
119	25	0.6	15	120	0.037	0.052
120	25	0.6	15	135	0.043	0.062
...
185	32.5	0.9	15	90	0.029	0.030
186	32.5	0.9	15	105	0.032	0.039
187	32.5	0.9	15	120	0.040	0.056
188	32.5	0.9	15	135	0.047	0.069
189	32.5	0.9	20	90	0.036	0.038
190	32.5	0.9	20	105	0.039	0.047
191	32.5	0.9	20	120	0.048	0.069
192	32.5	0.9	20	135	0.056	0.083

Table 5 Average single-abrasive-grain grinding forces of SiCp/Al composite under different working conditions

v_s (m/s)	v_w (m/min)	a_p (μm)	Total F_t (N)	Total F_n (N)	Average F_t' (N)	Average F_n' (N)
10	0.3	5	6.57	12.02	0.031	0.052
10	0.3	10	8.78	14.42	0.030	0.048
10	0.3	15	10.46	16.31	0.027	0.044
10	0.3	20	12.99	18.79	0.028	0.043
10	0.6	5	8.13	14.06	0.036	0.063
10	0.6	10	10.33	16.70	0.035	0.053
10	0.6	15	12.92	18.32	0.034	0.048
...
25	0.3	5	5.62	11.81	0.025	0.052
25	0.3	10	7.28	13.29	0.023	0.043
25	0.3	15	8.93	15.21	0.023	0.040
25	0.3	20	10.08	18.03	0.022	0.041
...
32.5	0.6	15	8.84	17.57	0.022	0.047
32.5	0.6	20	10.59	19.97	0.021	0.044
32.5	0.9	5	5.98	13.67	0.028	0.062
32.5	0.9	10	7.05	17.40	0.023	0.056
32.5	0.9	15	8.98	19.98	0.024	0.053
32.5	0.9	20	10.59	21.64	0.023	0.047

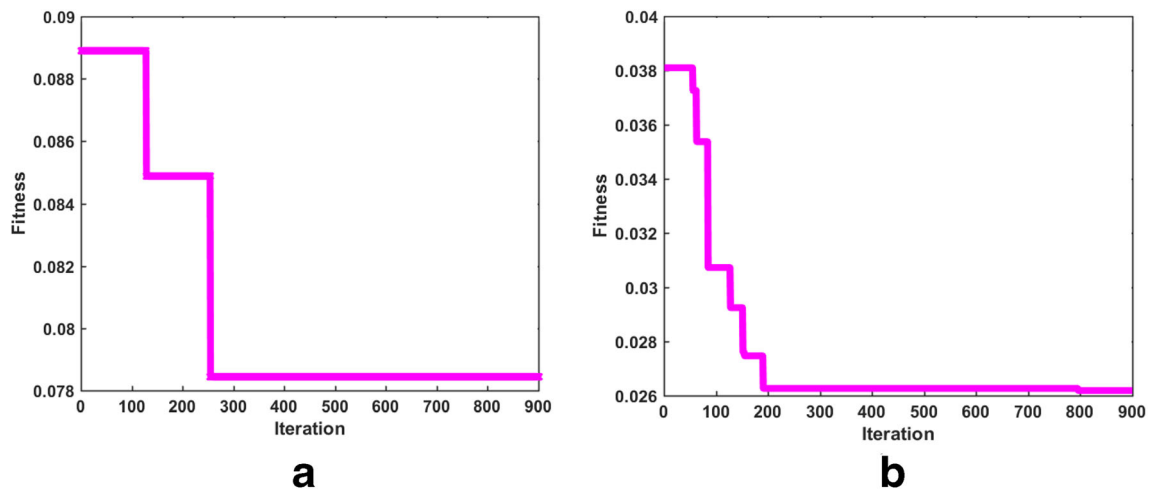


Fig. 14 Convergence graph of PSO-SVM prediction model. a Tangential grinding force. b Normal grinding force

In addition, the optimal parameters of the normal grinding force prediction model with single-abrasive grain can be computed:

$$g_2 = 0.026, \mu_2 = 49.79, \varepsilon_2 = 0.011.$$

Subsequently, the identified optimal parameters for the normal and tangential grinding forces are inserted into the SVM model.

3.3 Evaluation of grinding force prediction model of SiCp/Al composite

As shown in Table 6, eight groups of experiments were randomly chosen to evaluate the predicted results. The tangential force in the single-abrasive-grain grinding process predicted with the PSO-SVM agrees well with the experimental values; the relative errors are below 12% (Fig. 15a). In addition, the predicted and experimental normal forces agree well (Fig. 15b).

Table 6 Evaluation of grinding force prediction model of SiCp/Al composite

No.	v_s (m/s)	v_w (m/min)	a_p (μm)
1	18	0.6	8
2	18	0.5	10
3	20	0.6	8
4	18	0.2	6
5	24	0.6	8
6	18	0.4	4
7	30	0.6	8
8	18	0.9	12

4 Results and discussion

4.1 Influence of process parameters on single-abrasive-grain grinding force of SiCp/Al composite

The influence of different process parameters on the single-abrasive-grain grinding forces for abrasive grains with angles of 90° is presented in this section; Figs. 16 a–c present the relationships between the single-abrasive-grain grinding forces of the SiCp/Al composite and wheel speed, feed velocity, and grinding depth, respectively. For abrasive grains with an angle of 90° , the normal-to-tangential grinding ratio is approximately 1.

Evidently, the tangential and normal forces in the single-abrasive-grain grinding process decrease with increasing wheel speed and increase with increasing feed velocity and grinding depth. In addition, the predicted normal force and experimental results agree well.

4.2 Influence of grain angle on single-abrasive-grain grinding force of SiCp/Al composite

Figure 17 shows the influence of different grain angles on the single-abrasive-grain grinding forces of SiCp/Al composite. The normal-to-tangential grinding force ratio for a grain angle of 135° ranges between 1.8 and 2.4. When the grain angle is 120° , the normal-to-tangential grinding force ratio is approximately 1.5–1.8. Moreover, for a grain angle of 105° , the ratio is approximately 1.1–1.5. When the grinding depth is constant, the greater the grain angle is, the greater are the tangential force and single-abrasive-grain normal grinding force.

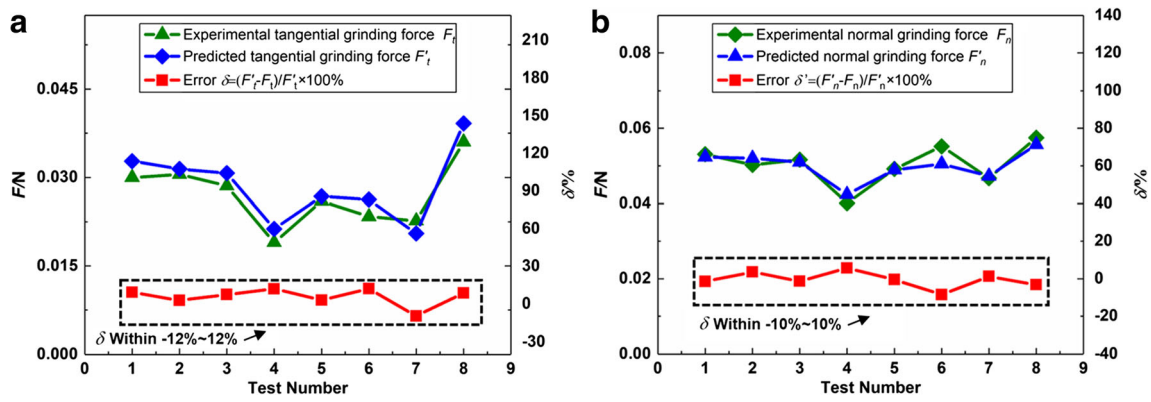


Fig. 15 Comparison of predicted and experimental single-abrasive-grain grinding forces. **a** Tangential grinding force. **b** Normal grinding force

4.3 Influence of process parameters on multi-abrasive-grain grinding force of SiCp/Al composite

Furthermore, the influences of the different process parameters on the grinding force were investigated. Figures 18 a–c show the relationships between the multi-abrasive-grain grinding forces and wheel speed, feed velocity, and grinding depth of SiCp/Al composite processing, respectively. The tangential and normal forces decrease with increasing wheel speed and

increase with increasing feed velocity and grinding depth. In addition, the normal multi-abrasive-grain grinding force of the SiCp/Al composite is slightly higher than the tangential grinding force (ratio of 1.2–2.2). In the single-abrasive-grain grinding experiments, the average angles of the abrasive grains range from 90° to 135° , and in the multi-abrasive-grain grinding experiments, the average angles of the abrasive grains range from 90° to 135° . In this grinding parameter range, the

Fig. 16 Influence of process parameters on single-abrasive-grain grinding force of SiCp/Al composite. **a** $v_w = 0.6$ m/min, $a_p = 0.1$ mm. **b** $v_s = 20$ m/s, $a_p = 0.1$ mm. **c** $v_s = 20$ m/s, $v_w = 0.6$ m/min

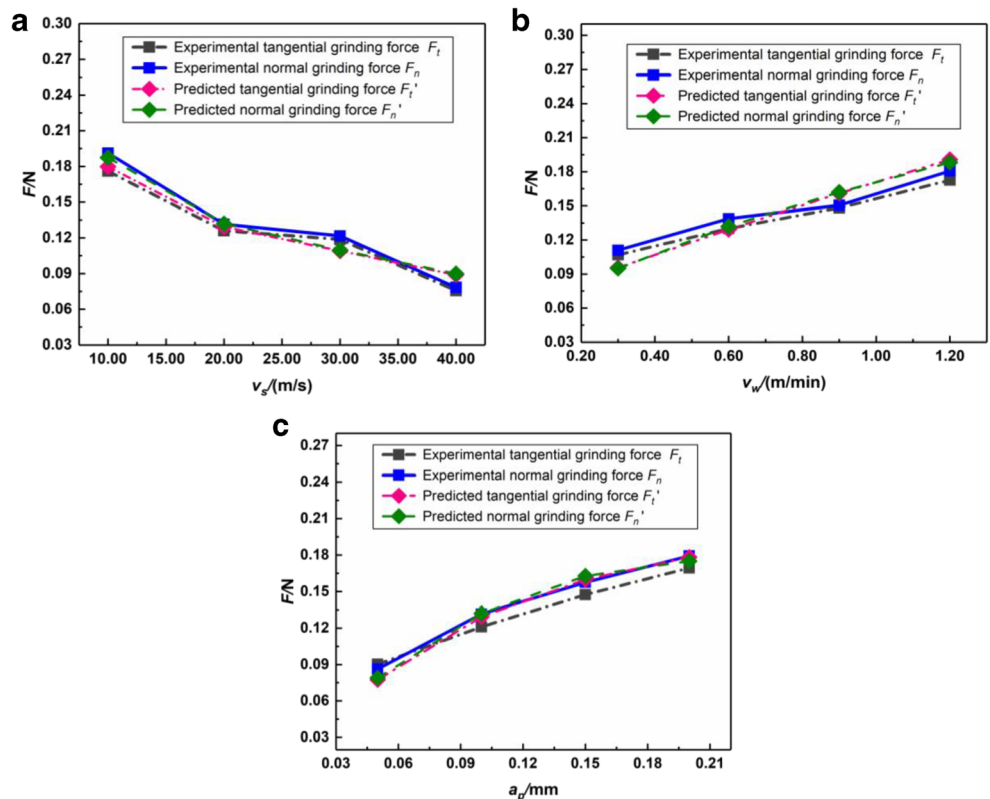
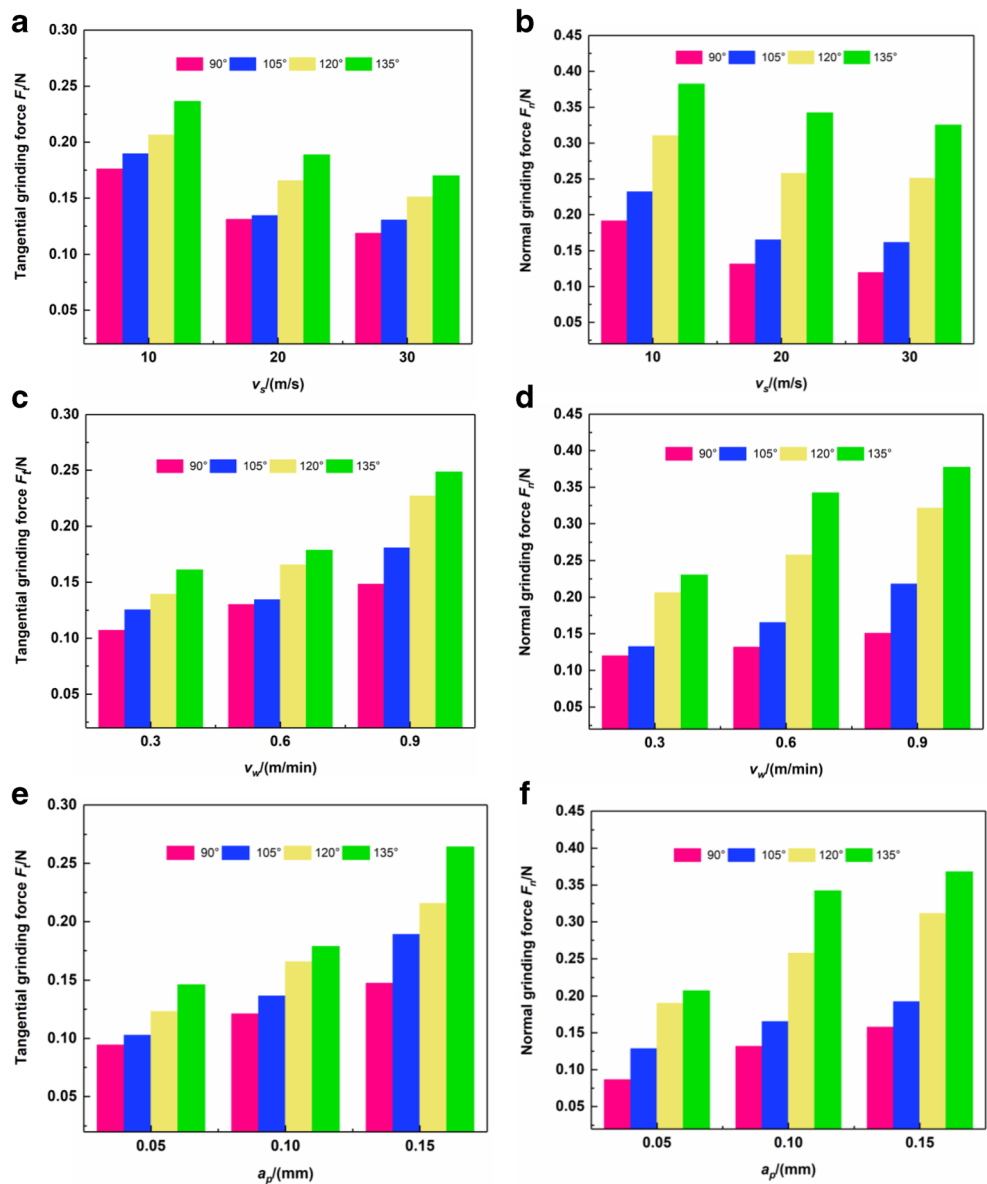


Fig. 17 Influence of grain angle on single-abrasive-grain grinding force of SiCp/Al composite. **a, b** $v_w = 0.6$ m/min, $a_p = 0.1$ mm. **c, d** $v_s = 20$ m/s, $a_p = 0.1$ mm. **e, f** $v_s = 20$ m/s, $v_w = 0.6$ m/min



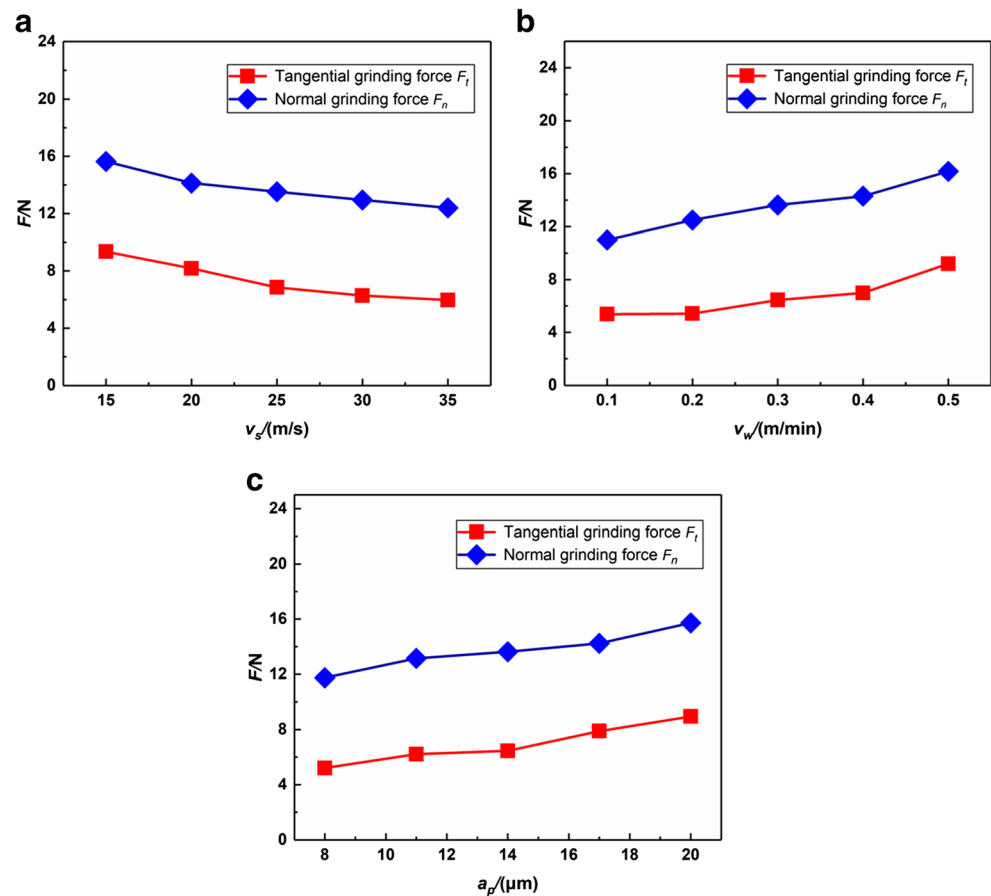
multi-abrasive-grain grinding force of the SiCp/Al composite changes only slightly.

4.4 Roles of theoretical model and PSO-SVM in the grinding force prediction model

Based on the idea of big data, grinding can be regarded as training a black box with several experiments. In the grinding process, the trained black box contains many unknown factors such as the abrasive-grain distribution, contact conditions, and dynamic effect. The grinding forces are considerably affected by the grinding grain angles. In this study, the abrasive-grain angle effect on the grinding force of SiCp/Al composite was considered. Therefore, the abrasive-grain angle was excluded from the black box.

The theoretical prediction model for the single-abrasive-grain grinding force for the abrasive-grain angle effect was established first. In the multi-abrasive-grain grinding experiments, the total abrasive grinding force can be obtained, and the average single-abrasive-grain grinding force can be calculated based on the number of abrasive grains. The grinding force of abrasive grains with angles of 90°, 105°, 120°, and 135° has a nonlinear relationship with the experimental average single-abrasive-grain grinding force. By adopting the PSO-SVM algorithm, the nonlinear relationship between the grinding force of abrasive grains with angles of 90°, 105°, 120°, and 135° and the experimental average single-abrasive-grain grinding forces was determined. Moreover, the forces measured at different single-grain grinding abrasive

Fig. 18 Influence of process parameters on multi-abrasive-grain grinding force of SiCp/Al composite. **a** $v_w = 0.6$ m/min, $a_p = 0.014$ mm. **b** $v_s = 25$ m/s, $a_p = 0.014$ mm. **c** $v_s = 25$ m/s, $v_w = 0.6$ m/min



grain angles were used as input to predict the total grinding force in the overall contact area.

For the traditional prediction model of grinding force, the input parameters are wheel speed, feed velocity, and grinding depth; here, the abrasive grain angle was considered and tried to make the grinding black box more clear. This method ensures better prediction precision than the traditional grinding force prediction model.

5 Conclusion

- (1) In this study, grinding experiments with single-abrasive grains on SiCp/Al composite were designed and conducted, and a prediction model for the single-abrasive-grain grinding force was developed to study the influence of the process parameters and grain angles on the grinding force of SiCp/Al composite.
- (2) Furthermore, multi-abrasive-grain grinding experiments were conducted under different grinding conditions to determine the multi-abrasive-grain grinding force, and a PSO-based SVM prediction method was used to establish a prediction model for the multi-abrasive-grain grinding force of SiCp/Al composite.

- (3) The error between the predicted and experimental grinding forces is below 12%. Thus, the grinding force prediction model based on the PSO–SVM algorithm can accurately predict grinding forces of SiCp/Al composite machining.
- (4) The prediction model for the grinding force of SiCp/Al composite provides theoretical support for the study of grinding micro-mechanisms.

6 Future work

In this study, single- and multi-abrasive-grain grinding experiments were conducted; in the latter case, the grinding process was regarded as a black box, which includes the dynamic effect and other grinding factors. The multi-abrasive-grain grinding force can be determined based on the single-abrasive-grain grinding force. In the future, the dynamic effect and other factors of the abrasive grain in the grinding process will be removed from the black box (such as the abrasive-grain angle in this study) to investigate the grinding processes of materials based on the geometric and dynamic effects more thoroughly.

Funding information This work was financially supported by the National Natural Science Foundation of China (Grant No. 51875413).

References

- Huang S, Guo L, He H, Yang H, Su Y, Xu L (2018) Experimental study on SiCp/Al composites with different volume fractions in high-speed milling with PCD tools [J]. *Int J Adv Manuf Technol* 97(5-8):2731–2739
- Huang S, Guo L, He H, Xu L (2018) Study on characteristics of SiCp/Al composites during high-speed milling with different particle size of PCD tools [J]. *Int J Adv Manuf Technol* 95:2269–2279
- Li J, Du J, Yao Y, Hao Z, Liu X (2014) Experimental study of machinability in mill-grinding of SiCp/Al composites [J]. *Journal of Wuhan University of Technology-Materials Science Edition* 29(6):1104–1110
- Han J, Hao X, Li L, Wu Q, He N (2017) Milling of high volume fraction SiCp/Al composites using PCD tools with different structures of tool edges and grain sizes [J]. *Int J Adv Manuf Technol* 92: 1875–1882
- Wang Y, Liao W, Yang K, Chen W, Liu T (2019) Investigation on cutting mechanism of SiCp/Al composites in precision turning [J]. *Int J Adv Manuf Technol* 100:963–972
- Hu F, Xie L, Xiang J, Umer U, Nan X (2018) Finite element modelling study on small-hole peck drilling of SiCp/Al composites [J]. *Int J Adv Manuf Technol* 96:3719–3728
- Xiang J, Xie L, Gao F, Yi J, Pang S, Wang X (2018) Diamond tools wear in drilling of Silicon carbide matrix composites containing copper [J]. *Ceram Int* 44(5):5341–5351
- Xiang J, Pang S, Xie L, Gao F, Hu X, Yi J, Hu F (2018) Mechanism-based FE simulation of tool wear in diamond drilling of SiCp/Al composites [J]. *Materials* 11(2):252–273
- Zhong Z, Hung N (2002) Grinding of alumina/aluminum composite [J]. *J Mater Process Technol* 123(1):13–17
- Ronald B, Vijayaraghavan L, Krishnamurthy R (2009) Studies on the influence of grinding wheel bond material on the grind ability of metal matrix composite [J]. *Mater Des* 30(3):679–686
- Shanawaz A, Sundaram S, Pillai U, Aurtherson P (2011) Grinding of aluminium silicon carbide metal matrix composite materials by electrolytic in-process dressing grinding [J]. *Int J Adv Manuf Technol* 57(1-4):143–150
- Huang S, Yu X (2017) A study of grinding forces of SiCp/Al composites [J]. *Int J Adv Manuf Technol* 4:1–7
- Zhou L, Huang S, Yu X (2014) Machining characteristic in cryogenic grinding of silicon carbide/Al composites [J]. *Acta Metallurgica Sin (English Letters)* 27(5):869–874
- Zha H, Feng P, Zhang J (2017) Experimental study on rotating ultrasonic milling of high volume fraction silicon carbide/Al composites [J]. *J Mech Eng* 53(19):107–113
- Liang G, Zhou X, Zhao F (2016) The grinding surface characteristics and evaluation of particle-reinforced aluminum silicon carbide [J]. *Sci Eng Compos Mater* 23(6):671–676
- Jia D, Li C, Zhang Y et al (2019) Experimental evaluation of surface topographies of NMQL grinding ZrO₂ ceramics combining multiangle ultrasonic vibration. *Int J Adv Manuf Technol* 100(1-4):457–473
- Gao T, Zhang X, Li C et al (2020) Surface morphology evaluation of multi-angle 2D ultrasonic vibration integrated with nanofluid minimum quantity lubrication grinding. *J Manuf Process* 51:44–61
- Yang M, Li C, Zhang Y (2019) et al. Predictive model for minimum chip thickness and size effect in single diamond grain grinding of zirconia ceramics under different lubricating conditions [J]. *Ceram Int* 45(12):14908–14920
- Yang M, Li C, Zhang Y (2019) et al. Effect of friction coefficient on chip thickness models in ductile-regime grinding of zirconia ceramics [J]. *Int J Adv Manuf Technol* 102(5):2617–2632
- Zhu C, Gu P, Liu D et al (2019) Evaluation of surface topography of SiCp/Al composite in grinding [J]. *Int J Adv Manuf Technol* 102: 2807–2821
- Zhu C, Gu P, Wu Y et al (2019) Surface roughness prediction model of SiCp/Al composite in grinding [J]. *Int J Mech Sci* 155: 98–109
- Younis M, Alawi H (1984) Probabilistic analysis of the surface grinding process [J]. *Trans CSME* 8(4):208–213
- Ren J, Hua D (1988) *Grinding principle* [M]. Northwestern Polytechnical University Press, Xian, pp 54–70
- Kishawy H, Kannan S, Balazinski M (2004) An energy based analytical force model for orthogonal cutting of metal matrix composites [J]. *CIRP Annual Manuf Technol* 53(1):90–94
- Sikder S, Kishawy H (2012) Analytical model for force prediction when machining metal matrix composite [J]. *Int J Mech Sci* 59(1): 95–103
- Zhou M, Zheng W (2016) A model for grinding forces prediction in ultrasonic vibration assisted grinding of SiCp/Al composites [J]. *Int J Adv Manuf Technol* 87:3211–3224
- Du J, Li J, Yao Y, Hao Z (2014) Prediction of cutting forces in mill-grinding SiCp/Al composites [J]. *Mater Manuf Process* 29(3):314–320
- Tohgo K, Itoh T (2005) Elastic and elastic-plastic singular fields around a crack-tip in particulate-reinforced composites with progressive debonding damage [J]. *Int J Solids Struct* 42(26):6566–6585
- Yu J, Hu Q, Wen Z, et al. Prediction model of surface roughness of 8418 steel by EDM based on SVM [J]. *China Mech Eng*, 2018, 4: 771-774.

Publisher's note Springer Nature remains neutral with regard to jurisdictional claims in published maps and institutional affiliations.